

KINEMATICS OF THE GALACTIC GLOBULAR CLUSTER SYSTEM: NEW RADIAL VELOCITIES FOR CLUSTERS IN THE DIRECTION OF THE INNER GALAXY

PATRICK CÔTÉ¹

California Institute of Technology, Mail Stop 105-24, Pasadena, CA 91125
 pc@astro.caltech.edu

Accepted for publication in the Astronomical Journal, August 1999 issue.

ABSTRACT

The High Resolution Echelle Spectrometer (HIRES) on the Keck I telescope has been used to measure the first radial velocities for stars belonging to eleven, heavily-reddened globular clusters in the direction of the inner Galaxy. The sample consists of the clusters Terzan 3, NGC 6256, IC 1257, NGC 6380 (= Ton 1), Ton 2 (= Pismis 26), Djorg 1, NGC 6540 (= Djorg 3), IC 1276 (= Pal 7), Terzan 12, NGC 6749 and Pal 10. Candidate cluster members were selected from a combination of previously published color-magnitude diagrams (CMDs) and new instrumental CMDs obtained with the Palomar 1.5m telescope. The systemic velocities of Djorg 1 and Pal 10 should be considered provisional since velocities are available for only two stars. For the remaining nine clusters, we have measured radial velocities for three to nine member stars. Using our HIRES spectra, we estimate metallicities of $[\text{Fe}/\text{H}] \simeq -0.75$ for both Terzan 3 and IC 1276: two cluster lacking previous metallicity estimates. The question of kinematic substructuring among the Galactic globular cluster system is investigated using an updated catalog of globular cluster distances, metallicities and velocities. It is found that the population of metal-rich globular clusters shows significant rotation at all Galactocentric radii. For the metal-rich clusters within 4 kpc of the Galactic center, the measured rotation velocity and line-of-sight velocity dispersion are similar to those of bulge field stars. We investigate claims that the metal-rich clusters are associated with the central Galactic bar by comparing the kinematics of the innermost clusters to that of the atomic hydrogen in the inner Galaxy. The longitude-velocity diagram of both metal-rich and metal-poor clusters bears a remarkable similarity to that of the gas, including the same non-circular motions which have traditionally been interpreted as evidence for a Galactic bar, or, alternatively, a non-axisymmetric bulge. However, uncertainties in the existing three-dimensional Galactocentric positions for most of the clusters do not yet allow an unambiguous discrimination between the competing scenarios of membership in a rigidly rotating bar, or in a bulge which is an oblate isotropic rotator. We conclude that the majority of metal-rich clusters within the central ~ 4 kpc of the Galaxy are probably associated with the bulge/bar, and not the thick disk.

Subject headings: Galaxy: globular clusters: general — Galaxy: structure — Galaxy: kinematics and dynamics — Galaxy: formation

1. INTRODUCTION

The spatial distribution, chemical abundance, age and kinematics of Galactic star clusters provide some of the most powerful constraints on models for the formation and evolution of the Milky Way. As the oldest and most metal-poor of these objects, globular clusters (GCs) have received particularly close scrutiny since their properties hold important clues to the structure and evolution of the Galaxy and its various components at the earliest possible epochs.

Most of the GCs within $\sim 25^\circ$ of the Galactic center have high metallicities relative to their counterparts at large Galactocentric distances. Although it has been recognized for some time that the Galactic GC system shows a bimodal distribution in metallicity (Morgan 1959; Kinman 1959), and that the metal-poor component is clearly associated with the Galactic halo, the proper categorization of the metal-rich GCs is less certain. Early suggestions that the metal-rich (*i.e.*, G-type) GCs formed a flattened, disk-like system (*e.g.*, Baade 1958; Morgan 1959; Kinman 1959) were called into question by Woltjer (1975), Harris (1976) and Frenk & White (1982) who

argued that these GCs followed a spherical (or at most slightly flattened) distribution which was more closely concentrated to the Galactic center than their metal-poor (F-type) counterparts. Later, Zinn (1985) and Armandroff (1989) suggested that the metal-rich GCs belonged to the thick disk, whereas Minniti (1995) argued, on the basis of improved metallicities and kinematics of bulge field stars, that most of the metal-rich GCs are in fact associated with the bulge. Using improved distances and metallicities for GCs within 5° of the Galactic center, Barbuy, Bica & Ortolani (1998) also suggested that these clusters belong to the bulge. Burkert & Smith (1997) have even proposed that the metal-rich GCs *themselves* show evidence for substructuring, and suggested that at least some of these metal-rich clusters are associated with a central Galactic bar.

Minniti (1995) considered several pieces of evidence which led him to suggest that most MR GCs belong not to the Galactic thick disk but, rather, to the bulge. First, and perhaps most importantly, the metal-rich GCs are *highly* concentrated to the Galactic center — more so than would be expected if they are associated with an exponen-

¹Sherman M. Fairchild Fellow

tial thick-disk having a scale-length of $h_r \sim 3$ kpc (*e.g.*, Ojha et al. 1996), yet consistent with that expected for a bulge-like density distribution (*e.g.* $\rho_b \propto R_G^{-m}$ where $3.65 \lesssim m \lesssim 4.2$; Terndrup 1988, Blanco & Terndrup 1989). Supporting evidence for the association of the metal-rich GCs with the bulge included the agreement between the mean metallicities for metal-rich GCs and bulge stars, and the similarity between the morphology of the CMDs for metal-rich GCs and those for the bulge field population (*e.g.*, Ortolani et al. 1995b). Minniti (1995) also considered the kinematic properties of the metal-rich GCs, although in this case the small number of GCs in the direction of the inner Galaxy having accurate velocities made it impossible to draw firm conclusions. For instance, in the most recent edition of the Milky Way GC Catalog (see Harris 1996),² roughly 15% of the GCs lack measured radial velocities. Many of these objects are low-concentration GCs in the direction of the inner Galaxy which suffer from heavy reddening and extreme crowding by field stars: characteristics which have precluded radial velocity measurements based on integrated-light spectroscopy.

In this paper, we report the first radial velocities for eleven GCs in the direction of the inner Galaxy, as well as approximate metallicities for two GCs lacking previous estimates. These data are supplemented with improved reddennings, metallicities and distances for many of the innermost Galactic GCs (Barbuy, Bica & Ortolani 1998; and references therein) in order to investigate the kinematics of the Galactic GC system and, in particular, to compare the kinematics of the metal-rich and metal-poor GC populations to those of the Galactic halo, disk and bulge components.

2. OBSERVATIONS AND REDUCTIONS

2.1. Target Selection

The eleven GCs targeted in this study are listed in Table 1. Since most of these clusters are located in crowded fields, it was necessary to select prospective cluster red giants based on their location in the color-magnitude diagram (CMD). In several cases, adequate CMDs are available in the literature (*i.e.*, NGC 6256, Alcaino 1983; NGC 6380 and Terzan 12, Ortolani, Bica & Barbuy 1998; Ton 2, Bica, Ortolani & Barbuy 1996; Djorg 1, Ortolani, Bica & Barbuy 1995a). For the remaining GCs, no suitable data could be found in the literature, and new multi-filter imaging was required.

We used the Palomar 1.5m telescope and direct CCD camera with a 2048×2048 detector (scale = $0''.37$ pixel⁻¹) with Johnson *V* and Kron *I* filters to obtain images of Terzan 3, IC 1257, NGC 6540, IC 1276 and Pal 10 on 1-2 June 1998. Both nights suffered from intermittent clouds, so candidate cluster members were selected from instrumental CMDs generated using the DAOPHOT II photometry package (Stetson 1993). For one additional cluster, NGC 6749, candidate member stars were selected from a *V*, *V* - *I* CMD constructed from archival CFHT images retrieved from the Canadian Astronomy Data Centre. Finding charts for these six GCs are shown in Figures 1-

6. All stars observed with HIRES are identified using the numbering scheme adopted in Table 1. For the remaining clusters, the identification numbers correspond to those of the photometric studies referenced in the final column of Table 1. When available, magnitudes and colors for these stars are recorded in columns 6-8.

2.2. HIRES Spectroscopy

We used the High Resolution Echelle Spectrometer (HIRES; Vogt et al. 1994) on 25-26 June 1998 to obtain high-resolution, low-S/N spectra for 54 candidate member red giants in the eleven GCs listed in Table 1. The 2048×2048 detector was binned 2×2 , and the lone read-out amplifier was adjusted to the high gain setting of $2.4 e^-/\text{ADU}$. The red collimator was used along with the cross-disperser in first order. The latter was adjusted to an angle of -0.2° which, combined with the adopted grating angle of 0.0° , yielded a spectral coverage of $4200 \lesssim \lambda \lesssim 6600 \text{ \AA}$. The C1 decker was used to limit to the entrance aperture to $0''.86 \times 7''.0$. Although conditions were photometric on both nights, the seeing was typically $\sim 1''.2$. Exposure times ranged from 60s to 1800s. Thorium-Argon comparison lamp spectra were taken immediately before and after each telescope movement, or roughly every hour in those cases where a particular GC was observed for an extended period.

The images were trimmed, overscan-corrected and bias-subtracted in the usual manner. As a first step in the removal of cosmic rays, the IRAF³ task COSMICRAY was run on the images. With the APALL task, six echelle orders spanning the range 4920 to 5350 \AA were then identified, traced and extracted using high-S/N spectra of radial velocity standard stars taken at the beginning of each night. The resulting traces were then used to extract all remaining spectra in an identical manner, with the sole difference that the recentering option in APALL was invoked to account for small drifts of the object spectra perpendicular to the dispersion axis. Th-Ar comparison spectra were extracted in the same manner, and a total of 22-31 emission lines per order were used to derive the best-fit coefficients of a sixth-order Legendre polynomial used to parametrize the dispersion solution.

Object spectra were dispersion corrected with the REF-SPEC and DISPCOR tasks, using the comparison lamps which bracketed each set of observations for a particular cluster. The rms scatter in the fitted dispersion solution was typically $\sim 0.03 \text{ \AA}$ with a dispersion of $4.0 \text{ km s}^{-1} \text{ pixel}^{-1}$ near 5175 \AA . Cosmic rays which survived the initial cleaning of the images were then removed by fitting a third-order spline to the processed spectra, replacing those points more than 4σ above the continuum with the appropriate value of the fitted continuum. Heliocentric radial velocities were then measured using the FXCOR task. After some experimentation, it was found that the highest cross-correlation peaks were found for the order spanning the region 5128-5196 \AA . As a result, the final radial velocity for each star represents the weighted mean of the derived radial velocities for this single order, using nine template spectra for five different radial velocity standards acquired

²The Catalog of Parameters for Milky Way Globular Clusters is available electronically at <http://physun.physics.mcmaster.ca/GC/mwgc.dat>.

³IRAF is distributed by the National Optical Astronomy Observatories, which are operated by the Association of Universities for Research in Astronomy, Inc., under contract to the National Science Foundation.

throughout the two-night run (*i.e.*, HD182572, HD186791, HD223311, HD107328 and HD90861).

The results are summarized in Table 1 which gives, for each cluster, the identification of all stars observed with HIRES, the exposure time and the measured heliocentric radial velocity, the heliocentric Julian date, V magnitude, $(B - V)$ and $(V - I)$ color for each star (if available), and the reference for the photometry.

3. SAMPLE PROPERTIES

3.1. *New Metallicities*

Although the spectra for the majority of our program objects are of low signal-to-noise (*i.e.*, $S/N \sim 5 \text{ pixel}^{-1}$), a small number of stars have $S/N \sim 10\text{--}15 \text{ pixel}^{-1}$. This is just adequate to measure equivalent widths for the strongest metallic absorption lines. The IRAF task SPLOT was therefore used to determine equivalent widths for the relatively strong and isolated Fe I lines at 5328.051, 5216.283, 5232.952, 5171.610 and 5339.937 Å for 22 member stars in Pal 10, Ton 2, IC 1257, NGC 6749, NGC 6540, Terzan 3 and IC 1276. For the last two clusters, there are no published metallicity estimates, so we used the empirical relation between mean equivalent width and published metallicity for Pal 10, Ton 2, IC 1257 and NGC 6749 to estimate $[\text{Fe}/\text{H}] \sim -0.75 \pm 0.25$ for both Terzan 3 and IC 1276 (see Figure 7). The quoted uncertainty reflects the observed scatter about the adopted relation, presumably due to neglecting the small differences in effective temperature and surface gravity among the calibrating stars (along with the uncertainties in the published cluster metallicities, most of which have been derived photometrically). During this exercise, we noticed that the equivalent widths of four stars in NGC 6540 appeared slightly lower than those expected for a cluster having metallicity $[\text{Fe}/\text{H}] = -1.0$, the value estimated for NGC 6540 by Bica et al. (1994) on the basis of $UBVI$ photometry and low-resolution, integrated-light spectroscopy. Given the crowded nature of this field, it is possible that the earlier estimate may have been biased upwards by interloping disk and bulge field stars. Based on the empirical relation shown in Figure 7, we estimate $[\text{Fe}/\text{H}] \simeq -1.40 \pm 0.25$ for NGC 6540.

3.2. *Observed and Derived Parameters for Program Clusters*

Table 2 gives a number of observed parameters for our eleven program GCs. From left to right, this table lists the cluster name, right ascension, declination, Galactic longitude and latitude, integrated V -band magnitude, reddening, concentration index and core radius. With the exception of the new and revised metallicities for the three GC discussed above, all of the data are taken from Barbuy et al. (1998) and the 1997 edition of the Milky Way GC Catalog of Harris (1996). Table 3 gives derived parameters for the same sample of GCs. Columns 1-7 record, from left to right, the cluster name, heliocentric distance, Galactocentric distance, rectangular coordinates in the system of Harris (1996) and metallicity (which, in almost every case, has been derived from the morphology of the observed CMD). Columns 8-10 give the number of stars found to be cluster members, the mean radial velocity of these stars and their intrinsic one-dimensional velocity dispersion. These

latter two quantities were calculated using the technique described in Suntzeff et al. (1993).

No velocity dispersion is reported for Djorg 1 and Pal 10 since only two radial velocities are available for stars in each of these clusters; in both cases, the measured pair of velocities are in excellent agreement, suggesting that both stars are bonafide cluster members. Nevertheless, given the severe crowding in these fields, we consider the systemic radial velocities for these clusters to be provisional, particularly that of Djorg 1 whose velocity with respect to a stationary observer at the location of the Sun (see §3.3) would be, if confirmed, the largest yet measured. Indeed, if we assume that Djorg 1 is currently at perigalacticon (*i.e.* $R_p = 2.4 \text{ kpc}$) then, for a logarithmic Galactic potential having a circular velocity of $v_c = 220 \text{ km s}^{-1}$, the corresponding apocentric distance is

$$R_a = R_p \exp(v_o^2/2v_c^2) \quad (1)$$

where v_o is the cluster space velocity. For $\bar{v}_r \leq v_o \lesssim \sqrt{3}\bar{v}_r$, the inferred apocentric distance falls in the range $10 \lesssim R_a \lesssim 140 \text{ kpc}$, which places Djorg 1 in the outer halo. This location seems incompatible with the published metallicity of $[\text{Fe}/\text{H}] = -0.4$ (Ortolani et al. 1995a) for this cluster; we note that the existing CMD for this cluster provides only weak constraints on the cluster metallicity, raising the possibility that Djorg 1 may be a misclassified MP halo cluster. Improved imaging of Djorg 1 and, especially, spectroscopy of additional candidate members are clearly warranted.

3.3. *Provisional Mass-to-Light Ratios*

Although radial velocities are available for only a small number of stars in each GC, the velocity precision is sufficiently high that it is possible to derive rough mass-to-light ratios for these GCs. Illingworth (1976) showed that the total mass for a GC can be expressed as

$$M = 167r_c\mu\sigma_0^2 \quad (2)$$

where r_c is the core radius in parsecs, μ is the dimensionless mass of the best-fit King model (King 1966) and σ_0 is the radial component of the central velocity dispersion. We approximate this latter quantity with σ_v (given in column 10 of Table 8). This is a reasonable approximation since most of our member stars are situated in the cores of their respective clusters. The final three columns of Table 8 record the total luminosities, total masses and mass-to-light ratios for the nine program clusters having three or more measured radial velocities. These mass-to-light ratios are, of course, highly uncertain owing to the small number of available velocities. Nevertheless, it is reassuring to note that the weighted mean for the sample is $M/L_V = 2.2 \pm 1.1$ in solar units: indistinguishable from the mass-to-light ratios found for nearby GCs using much larger samples of radial velocities (*e.g.*, Pryor & Meylan 1993).

4. KINEMATICS OF THE GALACTIC GLOBULAR CLUSTER SYSTEM

4.1. *Parsing the Sample on the Basis of Metallicity*

An outstanding question in GC research is the origin of the chemically-distinct GC populations associated

with many giant galaxies (see, *e.g.*, Ashman & Zepf 1992; Forbes, Brodie & Grillmair 1997; Côté, Marzke & West 1998). Central to this question are the issues of substructuring in the Galactic GC system and the proper categorization of the various GC subsystems with the Galactic halo, bulge/bar or thick disk. We regard the bimodal metallicity distribution of Galactic GCs the strongest single piece of evidence for the presence of distinct GC populations in the Milky Way. Thus, we proceed by first dividing the Galactic GC system into metal-rich and metal-poor components, and then analyzing their kinematics separately.

Figure 8 shows the metallicity distribution of 133 Galactic GCs having measured chemical abundances. The metallicities — which are essentially on the Zinn & West (1984) scale — are taken from the most recent version of the catalog of Harris (1996), supplemented with recent data from Barbuy et al. (1998) and with the metallicity estimates for Terzan 3, IC1276 and NGC 6540 presented in §3.1. The evidence for two distinct GC populations, first suggested by Morgan (1959), is immediately apparent as two peaks in the distribution. The double-Gaussian which best fits the observed data is shown by the solid line; the metal-poor (MP) and metal-rich (MR) components are indicated by the dotted lines. These Gaussians have parameters $N_{\text{mp}} = 14.9$ per 0.125 dex, $[\text{Fe}/\text{H}]_{\text{mp}} = -1.59$ dex and $\sigma_{\text{mp}} = 0.30$ dex for the MP component, and $N_{\text{mr}} = 7.1$ per 0.125 dex, $[\text{Fe}/\text{H}]_{\text{mr}} = -0.55$ dex and $\sigma_{\text{mr}} = 0.27$ dex for the MR component.

Most previous discussions concerning the proper categorization of these two GC populations have involved dividing the sample into two components at some intermediate metallicity. However, it is clear from Figure 8 that approach is likely result in the inclusion of some GCs in the MR component which are more properly associated with the MP GC population, and vice versa. In an attempt to avoid such complications, we choose to divide the sample into *three* components: (1) a sample of 31 MR GCs (including Djorg 1) having $[\text{Fe}/\text{H}] < -0.75$; (2) a sample of 82 MP GCs having $[\text{Fe}/\text{H}] \leq -1.29$ and; (3) a sample of 20 intermediate metallicity (IM) GCs having $-1.29 < [\text{Fe}/\text{H}] \leq -0.75$. Thus, although a mixture of MP and MR GCs are expected in the IM sample, the MR and MP samples should be relatively uncontaminated by interlopers.

4.2. Parametric Solutions for Velocity Dispersion and Rotational Velocity

We now investigate the kinematics of these three GC samples using familiar parametric techniques first described in Kinman (1959), Frenk & White (1980), Zinn (1985) and Hesser, Shawl & Meyer (1986). First, we consider the case of constant rotation velocity, v_r . A population of GCs having constant v_r should fall along a relation of the form

$$v_s = v_r \cos \psi + v_p \quad (3)$$

where v_s is the velocity with respect to a stationary observer at the location of the Sun, ψ is the angle between the rotational-velocity vector of the GC and the direction to the Sun, and v_p is the peculiar velocity of the GC with

respect to the derived solution. The angle ψ is given by

$$\cos \psi = \frac{R_\odot \cos A}{\sqrt{R_s^2 \cos^2 A + (R_\odot - R_s \cos b \cos l)^2}} \quad (4)$$

where R_\odot is the Galactocentric distance of the Sun (taken to be 8 kpc), R_s is the heliocentric distance of the GC, and l and b are its Galactic longitude and latitude.⁴ The angle A is the angle between the apex of the Local Standard of Rest (LSR) and the position of the GC on the sky, given by $\cos A = \sin l \cos b$. Thus, $v_s = v_{\text{lsr}} + 220 \cos A$ where v_{lsr} is the velocity with respect to the LSR.

A second, frequently-used rotation law is the case of solid-body rotation. In this instance, v_s is given by

$$v_s = \omega R_\odot \cos A + v_p \quad (5)$$

where ω is the angular velocity. The observed flat rotation curve of the thick disk (Ojha et al. 1996) suggests that equation 3 should provide an adequate description for the observed radial velocities of thick disk objects, although it is important to bear in mind that the available data are limited to the solar neighborhood (*i.e.*, there exist virtually no observational constraints on the kinematics of thick-disk stars within a few kpc of the Galactic center). On the other hand, equation 4 should give a superior representation for objects belonging to the Galactic bulge — an oblate isotropic rotator which is adequately described by solid-body rotation (Kent 1992; Ibata & Gilmore 1995; Tiede & Terndrup 1997).

We have derived the best-fit values of v_r , ω , and their associated line-of-sight velocity dispersions, σ_v and $\sigma_{\omega R_\odot}$, using various sub-samples of the Galactic GC population. The results of this exercise is summarized in Table 4, whose first four columns record the metallicity of the chosen GC sample (*i.e.*, MR, MP or IM), the range of Galactocentric radii spanned by these GCs, their mean Galactocentric radius, and the total number of objects in the sample. Columns 4-8 list the calculated values of v_r , σ_v , ω , σ_ω and the ratio of ordered-to-random motions, v_r/σ_v . The number given in the final column identifies the sample used in calculating the best-fit kinematic parameters. In addition to dividing the sample on the basis of metallicity, we have parsed the sample on the basis of Galactocentric radius by considering three different cases: (1) GCs interior to $R_G = 4$ kpc; (2) GCs beyond $R_G = 4$ kpc and; (3) all GCs, irrespective of distance from the Galactic center. Note that this choice of dividing radius, though arbitrary, corresponds roughly to the co-rotation radius of the Galactic bar observed in 3D N-body simulations (*e.g.*, 3-5 kpc; Fux 1997), the effective radius of the Galactic bulge (2.7 kpc; Gilmore, King & van der Kruit 1990) and the median *K*-band effective radius measured for the bulges of Sb and Sbc galaxies (*i.e.*, $\simeq 4$ kpc for $H_0 = 75 \text{ km s}^{-1} \text{ Mpc}^{-1}$; de Jong 1996). Roughly two-thirds (20/31) of the MR GCs (which span the range $0.6 \leq R_G \leq 7.6$ kpc with mean $\overline{R_G} = 3.2 \pm 2.0$ kpc) are located within 4 kpc of the Galactic center.

The results of this exercise are shown in Figures 9 and 10. The distribution of v_s with $\cos \psi$ for Galactic GCs is shown in Figure 9, whereas Figure 10 shows the distribu-

⁴Note that equation (2) of Burkert & Smith (1997) contains a typographical error. In their notation, R should denote the *heliocentric* distance of the cluster.

tion of v_s with $\cos A$. While most of the data used to construct these figures have been taken from of Harris (1996), we have added new velocities for the eleven GCs studies here and have made use of the improved radial velocities of seven outer halo GCs given in Djorgovski et al. (1999). In both figures, the upper panel shows the distribution for the MR GCs (circles); MP and IM GCs are plotted in the lower panel (squares and triangles, respectively). As described above, all three samples have been sub-divided on the basis of Galactocentric radius; open symbols refer to GCs located more than 4 kpc from the Galactic center, whereas GCs interior to this radius are plotted as filled symbols.

Also shown in Figures 9 and 10 are the best-fit relations of the form of equation 3 and 5, respectively. Each line is marked with the number given in the last column of Table 4, identifying the sample of GCs used in deriving the rotation solution (except for the lower panel of Figure 9 where the labels have been omitted for clarity). A number of conclusions may be drawn from these figures. First, the MR GCs show significant rotation at all radii.⁵ Second, only among the outermost MR GCs does the quantity v_r/σ_v substantially exceed unity, meaning that this component of the Galactic GC system is supported primarily by ordered, and not random, motions (Zinn 1985; Armandroff 1989). Third, the MP GCs as a whole show little or no evidence for rotation: a familiar result which is well established from earlier studies (*e.g.*, Kinman 1959; Frenk & White 1980; Zinn 1985; Hesser et al. 1986) although we note that there is some indication that the inner sample of MP GCs *may* be rotating slowly. Not surprisingly, the results for the IM sample are intermediate to those found for the MR and MP GCs: *i.e.*, rotation is generally significant at all radii, but of lower amplitude than for the sample of MR GCs. This is not unexpected since the sample IM GCs almost certainly represents an inhomogeneous mixture of the MR and MP samples.

4.3. Comparison to the Bulge Field Star Population

Is the observed rotation of MR GCs in the inner Galaxy more characteristic of the bulge or disk populations? The dashed lines in the upper and lower panels of Figure 11 show the bulge rotation law found by Tiede & Terndrup (1997) over the range $-10^\circ \leq l \leq 10^\circ$. The dotted lines which span the range $5^\circ \leq |l| \leq 25^\circ$ show the rotation law for the outer bulge measured by Ibata & Gilmore (1995) for $|b| \geq 12^\circ$, offset by $\pm 55 \text{ km s}^{-1}$ in order to match the relation of Tiede & Terndrup (1997) over the range $5^\circ \lesssim |l| \lesssim 10^\circ$. MR GCs are plotted in the upper panel; MP and IM GCs are given in the lower panel. As in the previous two figures, open symbols refer to GCs having $R_G > 4 \text{ kpc}$, while the filled symbols indicate objects with $R_G < 4 \text{ kpc}$. The errorbar in the upper panel shows the typical velocity dispersion of 110 km s^{-1} for bulge objects, as summarized in Table 1 of Kent (1992). This dispersion agrees closely with that found for the MR GCs in §4.2, particularly for those clusters with $R_G \leq 4 \text{ kpc}$. In addition, the agreement between the rotational laws for bulge stars and the MR GCs appears quite reasonable. Interestingly, the innermost MP and IM GCs also show reasonable agreement with rotation law deduced from observations of

bulge field stars.

4.4. Comparison to the HI Gas in the Inner Galaxy: Is there Evidence for Bar-like Kinematics?

Unfortunately, a direct comparison to the kinematics of the thick-disk field star population in the central few kiloparsecs of the Galaxy is not possible, as there exist no observational constraints on the kinematics of the thick-disk in this region. In fact, there are surprisingly few constraints on the kinematics of the *old thin disk* in the inner Galaxy, although it is thought that its velocity dispersion increases substantially within the central few kiloparsecs (*e.g.*, Lewis & Freeman 1989).

However, there do exist excellent observations of molecular and atomic gas in the inner Galaxy whose kinematics can be compared directly to that of the GCs. Figure 12 shows the well known longitude-velocity diagram for HI gas in the inner Galaxy based on 21 cm observations (*e.g.* Burton & Liszt 1993). Detailed discussions of the potential pitfalls involved in interpreting the gas kinematics may be found in Burton & Liszt (1993) and List (1992). Here, we simply summarize the two principal implications of these observations for Galactic structure models: (1) gas motions in the inner Galaxy deviate strongly from circularity; and (2) the origin of the non-circular motions may arise from the presence of a bar or a triaxial bulge potential in the inner Galaxy. The existence of a Galactic bar is now supported by much additional observational evidence, particularly COBE/DIRBE surface brightness maps of the inner Galaxy (Dwek et al. 1995; Binney, Gerhard & Spergel 1997), the asymmetric distribution of bulge red clump stars (Stanek et al. 1994; 1997) and the non-circular kinematics of ^{12}CO , ^{13}CO and CS gas (Bally et al. 1987; Dame et al. 1987; Binney et al. 1991).

The first claims of a bar-like (or highly flattened disk-like) feature in the spatial distribution of GCs were made by Baade (1958), Kinman (1959) and Morgan (1959). Woltjer (1975) and Harris (1976), however, cautioned that such a distribution might be due to the smearing effects of distance errors for low-latitude clusters in the direction of the Galactic center. Recently, the possibility that at least some of the MR GCs might be associated with a Galactic bar has been discussed by Burkert & Smith (1997) and Barbuy et al. (1998) who, using different samples, came to different conclusions. Using data from Harris (1996), Burkert & Smith (1997) argued that the highest-mass MR GCs fall along an elongated bar whose extent and orientation is consistent with that of the Galactic stellar bar. Barbuy et al. (1998), on the other hand, compared the spatial distribution of GCs found within 5° of the Galactic center to the outer contours of the Galactic bar proposed by Blitz & Spergel (1991), and concluded that the innermost GCs show no clear evidence for a bar. They note, however, that the solid angle spanned by their sample of clusters is sufficiently small that a bar-like distribution might be undetectable.

The velocity distribution of HI gas in the inner Galaxy, summed over the range $|b| \leq 1.5^\circ$, is shown by the contours in Figure 12. The innermost MR GCs (circles), MP GCs (squares) and IM GCs (triangles) are overlaid for compar-

⁵We omit Djorg 1 from the MR sample since its radial velocity and metallicity are uncertain; including it increases the derived rotation velocity and line-of-sight velocity dispersion for the sample of inner MR GCs by $\sim 15\%$ and 20% , respectively (see Table 4).

ison. Although the combined GC sample spans the range $|b| \lesssim 23^\circ$ (with mean $\bar{b} = 0.7^\circ \pm 9.2^\circ$), there is a striking agreement between the kinematics of the GCs and the atomic gas. Perhaps surprisingly, this is true of the entire sample of GCs, irrespective of metallicity. In the region of Galactic longitude spanned by the HI observations, there is only a single GC having $R_G < 4$ kpc which falls outside of the envelope defined by the HI gas. This object (located at $l \simeq 8$ and $v_{\text{lsr}} \simeq 200$ km s $^{-1}$) is NGC 6144: a poorly-studied GC whose Galactocentric distance of 3.4 kpc is based on a single photographic CMD (Alcaino 1980). An improved estimate of the distance of this cluster is desirable. Finally, we note that the pattern speed of the Galactic stellar bar, according to the dynamical models of Zhao (1996), is $\Omega_p \sim 60$ km s $^{-1}$ kpc $^{-1}$. To within the rather large uncertainties, this value is consistent with the angular velocity of $\omega = 43.6 \pm 22.3$ km s $^{-1}$ kpc $^{-1}$ found for the MR GCs within 4 kpc of the Galactic center.

4.5. Whence the Metal-Rich Globular Clusters?

The similarity between the longitude-velocity diagram of GCs and HI gas shown in Figure 12 is intriguing, but does it necessarily imply that the GCs are associated with the Galactic bar? Although it is notoriously difficult to distinguish motion along a dynamically cold bar from motion within a rigidly-rotating, elongated bulge having a significant velocity dispersion, one possible observational test of these different scenarios would be the existence of a distance-velocity relation among GCs: *i.e.*, if the GCs are indeed associated with the Galactic bar, then the position of each GC in the X-Y plane of the Galaxy should correspond uniquely to an observed radial velocity, something which is *not* true should they belong to a triaxial bulge. Figure 13 shows the Galactocentric XY coordinates of the all GCs within 4 kpc of the Galactic center. The large circle indicates the approximate co-rotation radius of the Galactic bar (Fux 1997), while the dotted lines show the limits placed on the orientation of the bar by observations of red clump giants (Stanek et al. 1997). In this figure, open symbols indicate clusters having $v_{\text{lsr}} \geq 0$ km s $^{-1}$ while filled symbols refer to GCs with $v_{\text{lsr}} < 0$ km s $^{-1}$. The bar-like feature noted by earlier workers is readily apparent, although it is clear that the XY positions of the GCs do not map uniquely into positive or negative velocities, as might be expected in bar models (see, *e.g.*, Figure 12 of Roberts et al. 1979). It is important to bear in mind, however, that the three-dimensional Galactocentric positions for many of these GCs remain sufficiently uncertain that definite conclusions regarding their possible association with the Galactic bar are premature. Improved distances for these heavily-obscured GCs, preferably based on deep infrared CMDs (*e.g.*, Kuchinski et al. 1995; Minniti et al. 1995), are needed to settle the issue.

The situation can be summarized as follows. Based on the evidence for rotation among the inner MR GCs, the close agreement between the overall rotation of the MR GC system and that of the bulge field stars, and the agreement between the kinematics of the innermost GCs and that of the HI gas, we suggest that majority of the MR GCs within 4 kpc of the Galactic center are more properly categorized as members of the Galactic bulge and/or bar (and not the thick disk), as suggested by Harris (1976) and re-emphasized by Minniti (1995). We caution, however, that

this simple interpretation (*i.e.*, the association of the innermost MR GCs with the bulge/bar) need not have been true at all times. For instance, some dynamical models for the formation of galactic bulges suggest that disk formation predates that of the bulge. Such models include bulge formation during the dissolution of bars which themselves form via disk instabilities (Hohl 1971) and the growth of bulges through the accretion of satellites onto disk galaxies (see, *e.g.*, Pfenniger 1993). Although the extremely old ages measured for MR clusters and bulge field stars (*e.g.* Ortolani et al. 1995b; Frogel 1998) may present difficulties for models in which the present population of MR GCs were initially associated with the inner regions of a disk system which ultimately became bar-unstable, additional observations (particularly improved ages for the innermost MR GCs and the thick-disk/bulge field star populations) are needed before such scenarios can be confirmed or ruled out.

5. SUMMARY

We have presented the first radial velocities for eleven, heavily-reddened GCs in the direction of the inner Galaxy. For two of these clusters (Pal 10 and Djorg 1), the velocities should be considered provisional due to the small number of stars observed. From the HIRES spectra used to measure these velocities, we estimate $[\text{Fe}/\text{H}] \simeq -0.75$ for Terzan 3 and IC 1276: two clusters lacking previous metallicity estimates. We have estimated provisional mass-to-light ratios for nine of the GCs; the mean of $\overline{M/L_V} = 2.2 \pm 1.1 M_\odot/L_{V,\odot}$ is similar to that found for nearby, well-studied clusters (*e.g.*, Pryor & Meylan 1993).

Using an updated catalog of GC positions, distances, metallicities and radial velocities we have investigated the kinematic properties of the MR and MP components of the Galactic GC system. The outermost MP GCs, and the MP GC population as a whole, shows little or no evidence for significant rotation, as expected for a system of halo objects. On the other hand, there may be some evidence that the innermost MP GCs are rotating slowly. We find that the MR GCs exhibit significant rotation at all radii, although rotation is dynamically important only among the outermost MR GCs. The rotation curve and line-of-sight velocity dispersion for the MR GCs within $\simeq 4$ kpc of the Galactic center shows good agreement with that observed for bulge stars. A comparison of the longitude-velocity diagram for all GCs with $R_G \lesssim 4$ kpc shows a remarkable similarity to that of the HI gas in the inner Galaxy, including the same non-circular motions which are often interpreted as evidence for a Galactic bar, or alternatively, an non-axisymmetric bulge. When improved three-dimensional Galactocentric positions become available for many GCs in the inner Galaxy, it may be possible to distinguish between these competing scenarios.

The author wishes to thank Wal Sargent for allocating two nights of unassigned Keck time to this project, George Djorgovski for his assistance during the observing run, Harvey Liszt for providing the HI data shown in Figure 12, and Steve Vogt for building such a magnificent instrument. Thanks also to John Blakeslee, Bill Harris, Sterl Phinney and Bob Zinn for helpful comments on earlier versions of this paper. The author gratefully ac-

knowledge support provided by the Sherman M. Fairchild Foundation. This study has made use of the Canadian Astronomy Data Centre, which is operated by the Herzberg Institute of Astrophysics, National Research Council of Canada.

TABLE 1
RADIAL VELOCITIES FOR GLOBULAR CLUSTER RED GIANT CANDIDATES

Cluster	Star	T (sec)	v_r (km s ⁻¹)	HJD (2440000+)	V (mag)	$(V - I)$ (mag)	$(B - V)$ (mag)	Reference
Terzan 3	1	180	-133.47±0.20	10990.7699				
	3	240	-137.43±0.19	10990.7813				
	4	240	-136.05±0.18	10990.7861				
	5	240	-133.70±0.23	10990.7939				
	6	240	-138.23±0.29	10990.7899				
	7	420	-137.94±0.23	10990.7992				
	8	420	20.30±0.19	10990.8052				
	9	420	-138.60±0.24	10990.8113				
	10	420	-136.19±0.25	10990.8173				
NGC 6256	1-5	90	-100.53±0.47	10990.8722	15.29		2.43	1
	1-8	150	-104.25±0.39	10990.8748	15.71		2.54	1
	1-11	150	-92.17±0.38	10990.8783	15.62		2.63	1
	1-14	150	-102.49±0.38	10990.8695	15.66		2.49	1
	1-13	210	-101.65±0.36	10990.8819	15.94		2.43	1
	1-39	300	-96.72±0.37	10990.8861	16.20		2.15	1
	1-20	420	-101.33±0.34	10990.8914	16.23		2.36	1
	13 ^a	420	-98.83±0.31	10990.8984				
IC 1257	1-19	420	-82.36±1.29	10990.9043	15.72		1.89	1
	1	1000	-141.79±0.40	10991.7681				
	2	750	-137.64±0.95	10991.7823				
	3	900	-131.41±1.03	10991.7935				
	4	1200	-140.93±1.30	10991.8266				
NGC 6380	5	1500	-140.91±1.11	10991.8092				
	977	1800	-0.01±0.87	10991.8532	18.30	2.93		2
	894	1500	-0.42±0.69	10990.9304	18.33	2.72		2
	1066	1500	-7.24±0.56	10990.9507	18.28	2.78		2
Ton 2	3258	900	-181.75±0.70	10990.9952	17.47	2.77		3
	3633	900	-187.81±0.34	10990.9709	17.03	3.17		3
	3644	900	-181.10±0.37	10990.9833	17.13	3.00		3
Djorg 1	330	1800	-364.30±0.69	10991.9352	18.26	3.40		4
	372	1800	-357.63±1.09	10991.8892	18.58	3.62		4
NGC 6540	12	60	-21.08±0.48	10991.0073				
	16	90	-20.19±0.44	10991.0096				
	27	120	-12.73±0.41	10991.0221				
	31	90	-21.43±0.70	10991.0144				
	57	120	-18.14±0.48	10991.0194				
	62	90	-16.96±0.33	10991.0120				
IC 1276	2	120	157.02±0.42	10991.0283				
	3	210	153.56±0.27	10991.0314				
	4	270	152.30±0.32	10991.0353				
	5	360	155.15±0.23	10991.0400				
	6	420	-12.16±0.24	10991.0458				
	10	420	159.86±0.25	10991.0518				
Terzan 12	294	1800	91.70±0.68	10992.0617	18.95	3.94		2
	410	1200	95.19±0.66	10992.0235	18.33	4.39		2
	428	1500	96.75±1.01	10992.0407	18.75	4.25		2
NGC 6749	1	300	-60.55±0.47	10992.0787				
	2	300	-60.00±1.05	10992.0836				
	3	420	-56.60±1.39	10992.0891				
	4	750	-71.36±0.76	10992.0973				
	5	750	-54.85±0.94	10992.1072				
	6	750	52.01±0.57	10992.1170				
Pal 10	1	1500	-31.21±0.35	10991.1105				
	5	1500	-32.09±0.31	10991.0922				

^aStar located 8''6 south and 6''2 west of star 1-20. REFERENCES: (1) Alcaïno 1983; (2) Ortolani, Bica & Barbuy 1998; (3) Bica, Ortolani & Barbuy 1996; (4) Ortolani, Bica & Barbuy 1995a.

TABLE 2
OBSERVED PARAMETERS FOR PROGRAM CLUSTERS

Cluster	$\alpha(2000)$ (h m s)	$\delta(2000)$ ($^{\circ}$ $'$ $''$)	l (deg)	b (deg)	V_T (mag)	$E(B - V)$ (mag)	c	r_c (arcmin)
Terzan 3	16:28:40.1	-35:21:13	345.1	9.2	12.00	0.32	0.70	1.18
NGC 6256	16:59:32.6	-37:07:17	347.8	3.3	11.29	0.84	2.50	0.02
IC 1257	17:27:08.5	-07:05:35	16.5	15.1	13.10	0.73	2.24	0.05
NGC 6380	17:34:28.0	-39:04:09	350.2	-3.4	11.31	1.07	1.55	0.34
Ton 2	17:36:10.5	-38:33:12	350.8	-3.4	12.24	1.26	1.30	0.54
Djorg 1	17:47:28.3	-33:03:56	356.7	-2.5	13.60	1.70	1.50	0.50
NGC 6540	18:06:08.6	-27:45:55	3.3	-3.3	9.30	0.60	2.50	0.03
IC 1276	18:10:44.2	-07:12:27	21.8	5.7	10.34	0.92	1.29	1.08
Terzan 12	18:12:15.8	-22:44:31	8.4	-2.1	15.63	2.06	0.57	0.83
NGC 6749	19:05:15.3	+01:54:03	36.2	-2.2	12.44	1.50	0.83	0.77
Pal 10	19:18:02.1	+18:34:18	52.4	2.7	13.22	1.66	0.58	0.81

TABLE 3
DERIVED PARAMETERS FOR PROGRAM CLUSTERS

Cluster	R_{\odot} (kpc)	R_G (kpc)	X (kpc)	Y (kpc)	Z (kpc)	[Fe/H] (dex)	N_*	\bar{v}_r (km s $^{-1}$)	σ_v (km s $^{-1}$)	L_V ($10^3 L_{\odot,V}$)	M ($10^3 M_{\odot}$)	M/L_V ($M_{\odot}/L_{\odot,V}$)
Terzan 3	26.4	18.9	-17.2	-6.7	4.2	-0.75	8	-136.3 \pm 0.7	1.9 \pm 0.5	23.6	28.8	1.2 \pm 0.6
NGC 6256	9.3	2.3	-1.1	-2.0	0.5	-1.01	9	-99.5 \pm 2.4	4.1 \pm 1.0	24.9	30.3	1.2 \pm 0.6
IC 1257	24.5	17.3	-14.6	6.7	6.4	-1.70	5	-140.2 \pm 2.1	3.4 \pm 1.1	23.6	83.7	3.5 \pm 2.2
NGC 6380	9.8	2.4	-1.6	-1.7	-0.6	-0.50	3	-3.6 \pm 2.5	4.2 \pm 1.7	52.0	83.0	1.6 \pm 1.3
Ton 2	6.4	2.0	1.7	-1.0	-0.4	-0.60	3	-184.4 \pm 2.2	4.0 \pm 1.6	16.3	46.9	2.9 \pm 2.4
Djorg 1	5.6	2.4	2.4	-0.3	-0.2	-0.40	2	-362.4 \pm 3.6		12.5		
NGC 6540	3.0	5.0	5.0	0.2	-0.2	-1.40	6	-17.7 \pm 1.4	3.1 \pm 0.9	8.2	8.7	1.1 \pm 0.6
IC 1276	9.3	3.6	-0.6	3.5	0.9	-0.75	5	155.7 \pm 1.3	3.0 \pm 1.0	74.5	75.5	1.0 \pm 0.6
Terzan 12	3.4	4.6	4.6	0.5	-0.1	-0.50	3	94.1 \pm 1.5	2.3 \pm 0.9	2.1	2.9	1.4 \pm 1.1
NGC 6749	7.7	4.9	1.8	4.6	-0.3	-1.60	5	-61.7 \pm 2.9	5.7 \pm 1.8	38.7	63.3	1.6 \pm 1.0
Pal 10	5.8	6.4	4.5	4.6	0.3	-0.10	2	-31.7 \pm 0.4		16.9		

TABLE 4
ROTATION SOLUTIONS FOR GALACTIC GC SUBSAMPLES

Sample	R_G (kpc)	$\overline{R_G}$ (kpc)	N	v_r (km s ⁻¹)	σ_v (km s ⁻¹)	ω (km s ⁻¹ kpc ⁻¹)	$\sigma_{\omega R_\odot}$ (km s ⁻¹)	v_r/σ_v	ID
MR ^a	>0	3.2	30	105±28	100	30.3± 6.8	94	1.0	1
	0-4	1.9	19	63±41	110	43.6±22.3	107	0.6	2
	≥4	5.4	11	157±28	67	28.5± 5.3	70	2.3	3
MP	>0	16.2	82	40±26	124	4.7± 3.7	125	0.3	4
	0-4	2.3	23	68±43	128	19.1±20.8	133	0.5	5
	≥4	21.6	59	22±33	123	4.2± 3.7	122	0.2	6
IM	>0	5.9	20	79±38	100	11.6± 8.9	106	0.8	7
	0-4	2.1	11	87±41	88	41.7±16.5	83	1.0	8
	≥4	10.6	9	64±76	118	5.0±11.3	121	0.5	9
MR ^b	>0	3.2	31	110±32	117	31.1± 8.1	113	0.9	
	0-4	2.0	20	72±50	135	50.5±27.2	130	0.5	
	≥4	5.4	11	157±28	67	28.5± 5.3	70	2.3	

^aExcluding Djorg1

^bIncluding Djorg1

REFERENCES

- Alcaino, G. 1980, *A&AS*, 39, 315
 Alcaino, G. 1983, *A&AS*, 53, 47
 Armandroff, T.E. 1989, *AJ*, 97, 375
 Ashman, K.A., & Zepf, S.E. 1992, *ApJ*, 384, 50
 Baade, W. 1958, in *Stellar Populations*, ed. D.K.J. O'Connell (North Holland, Amsterdam), p. 303
 Bally, J., Stark, A.A., Wilson, R.W., & Henkel, C. 1987, *ApJS*, 65, 13
 Barbuy, B., Bica, E., & Ortolani, S. 1998, *A&A*, 333, 117
 Bica, E., Ortolani, S., & Barbuy, B. 1994, *A*, 283, 67
 Bica, E., Ortolani, S., & Barbuy, B. 1996, *A&AS*, 120, 153
 Binney, J., Gerhard, O.E., & Spergel, D. 1997, *MNRAS*, 288, 365
 Binney, J., Gerhard, O.E., Stark, A.A., Bally, J., & Uchida, K.I. 1991, *MNRAS*, 252, 210
 Blanco, V.M. & Terndrup, D.M. 1989, *AJ*, 98, 843
 Blitz, L., & Spergel, D. 1991, *ApJ*, 379, 631
 Burkert, A., & Smith, G.H. 1997, *ApJ*, 474, 15
 Burton, W.B., & Liszt, H.S. 1993, *A&A*, 274, 765
 Côté, P., Marzke, R.O., & West, M.J. 1998, *ApJ*, 501, 554
 Dame, T.M., Ungerechts, H., Cohen, R.S., de Grus, E.J., Grenier, I.A., May, J., Murphy, D.C., Nyman, L.-A., & Thaddeus, P. 1987, *ApJ*, 322, 706
 de Jong, R.S. 1996, *A&A*, 313, 45
 Djorgovski, S.G., Côté, P., Meylan, G., & McCarthy, J.K., 1999, in preparation.
 Dwek, E., Arendt, R.G., Hauser, M.G., Kelsall, T., Lisse, C.M., Moseley, S.H., Silverberg, R.F., Sodroski, T.J., & Weiland, J.L. 1995, *ApJ*, 445, 716
 Forbes, D.A., Brodie, J.P., & Grillmair, C.J. 1997, *AJ*, 113, 1652
 Frenk, C.S., & White, S.D.M. 1980, *MNRAS*, 193, 295
 Frenk, C.S., & White, S.D.M. 1982, *MNRAS*, 198, 173
 Frogel, J.A. 1998, in *Galaxy Evolution: Connecting the Distant Universe with the Local Fossil Record*, in press.
 Fux, R. 1997, *A&A*, 327, 983
 Gilmore, G., King, I.R., & van der Kruit, P.C. 1990, *The Milky Way as a Galaxy* (University Science Books, Mill Valley).
 Harris, W.E. 1976, *AJ*, 81, 1095
 Hesser, J.E., Shawl, S.J., & Meyer, J.E. 1986, *PASP*, 98, 403
 Hohl, F. 1971, *ApJ*, 168, 343
 Ibata, R., & Gilmore, G. 1995, *MNRAS*, 275, 605
 Illingworth, G.D. 1976, *ApJ*, 204, 73
 Kent, S.M. 1992, *ApJ*, 387, 181
 King, I.R. 1996, *AJ*, 71, 64
 Kinman, T.D. 1959, *MNRAS*, 119, 559
 Kuchinski, L.E., Frogel, J.A., Terndrup, D.M., & Perrson, S.E. 1995, *AJ*, 109, 1131
 Lewis, J.R., & Freeman, K.C. 1989, *AJ*, 97, 139
 Liszt, H.S. 1992, in *The Center, Bulge, and Disk of the Milky Way*, ed. L. Blitz (Dordrecht, Kluwer), p. 111
 Minniti, D. 1995, *AJ*, 109, 1663
 Minniti, D., Olszewski, E.W., & Rieke, M. 1995, *AJ*, 110, 1699
 Morgan, W.W. 1959, *AJ*, 64, 432
 Ojha, D.K., Bienaymé, Robin, A.C., Crezé, M., & Hohan, V. 1995, *A&A*, 311, 456
 Ortolani, S., Bica, E., & Barbuy, B. 1995a, *A&A*, 296, 680
 Ortolani, S., Bica, E., & Barbuy, B. 1997, *A&AS*, 126, 319
 Ortolani, S., Bica, E., & Barbuy, B. 1998, *A&AS*, 127, 471
 Ortolani, S., Renzini, A., Gilmozzi, R., Marconi, G., Barbuy, B., Bica, E., & Rich, R.M. 1995b, *Nature*, 377, 701
 Pfenniger, D. 1993, in *Galactic Bulges*, IAU Symposium 153, ed. H. Dejonghe & H.J. Habing, (Dordrecht, Kluwer), 387
 Pryor, C., & Meylan, G. 1993, in *The Structure and Dynamics of Globular Clusters*, ed. S.G. Djorgovski and G. Meylan (ASP, San Francisco), p. 357
 Roberts, W.W., Huntley, J.M. & van Albada, G.D. 1979, *ApJ*, 233, 67
 Stanek, K.Z., Mateo, M., Udalski, A., Szymanski, M., Kaluzny, J., & Kubiak, M. 1994, *ApJ*, 429, L73
 Stanek, K.Z., Udalski, A., Szymanski, M., Kaluzny, J., Mateo, M., & Krzemiński, W. 1997, *ApJ*, 477, 163
 Stetson, P.B. 1993, in *Stellar Photometry: Current Techniques and Future Developments*, IAU Coll. 136, ed. C.J. Butler & I. Elliot (Cambridge University Press, Cambridge), 291
 Suntzeff, N.B., Mateo, M., Terndrup, D.M., Olszewski, E.W., Geisler, D., & Weller, W. 1993, *ApJ*, 418, 208
 Tiede, G.P. & Terndrup, D.M. 1997, *AJ*, 113, 321
 Terndrup, D.M. 1988, *AJ*, 96, 884
 Vogt, S.S., et al. 1994, *SPIE*, 2198, 362
 Woltjer, L. 1975, *A&A*, 42, 109
 Zhao, H. 1996, *MNRAS*, 283, 149
 Zinn, R. 1985, *ApJ*, 293, 424
 Zinn, R., & West, M.J. 1984, *ApJS*, 55, 45

FIG. 1.— V-band finding chart for Terzan 3. This image measures $6'3 \times 6'3$. North is up and east is to the left. The numbering scheme is the same as that of Table 1.

FIG. 2.— V-band finding chart for IC 1257. This image measures $1'5 \times 1'5$. North is up and east is to the left. The numbering scheme is the same as that of Table 1.

FIG. 3.— V-band finding chart for NGC 6540. This image measures $1'5 \times 1'5$. North is up and east is to the left. The numbering scheme is the same as that of Table 1.

FIG. 4.— V-band finding chart for IC 1276. This image measures $3'0 \times 3'0$. North is up and east is to the left. The numbering scheme is the same as that of Table 1.

FIG. 5.— V-band finding chart for NGC 6749. This image, taken from the CFHT archive, measures $1'5 \times 1'5$. North is up and east is to the left. The numbering scheme is the same as that of Table 1.

FIG. 6.— V-band finding chart for Pal 10. This image measures $3'0 \times 3'0$. North is up and east is to the left. The numbering scheme is the same as that of Table 1.

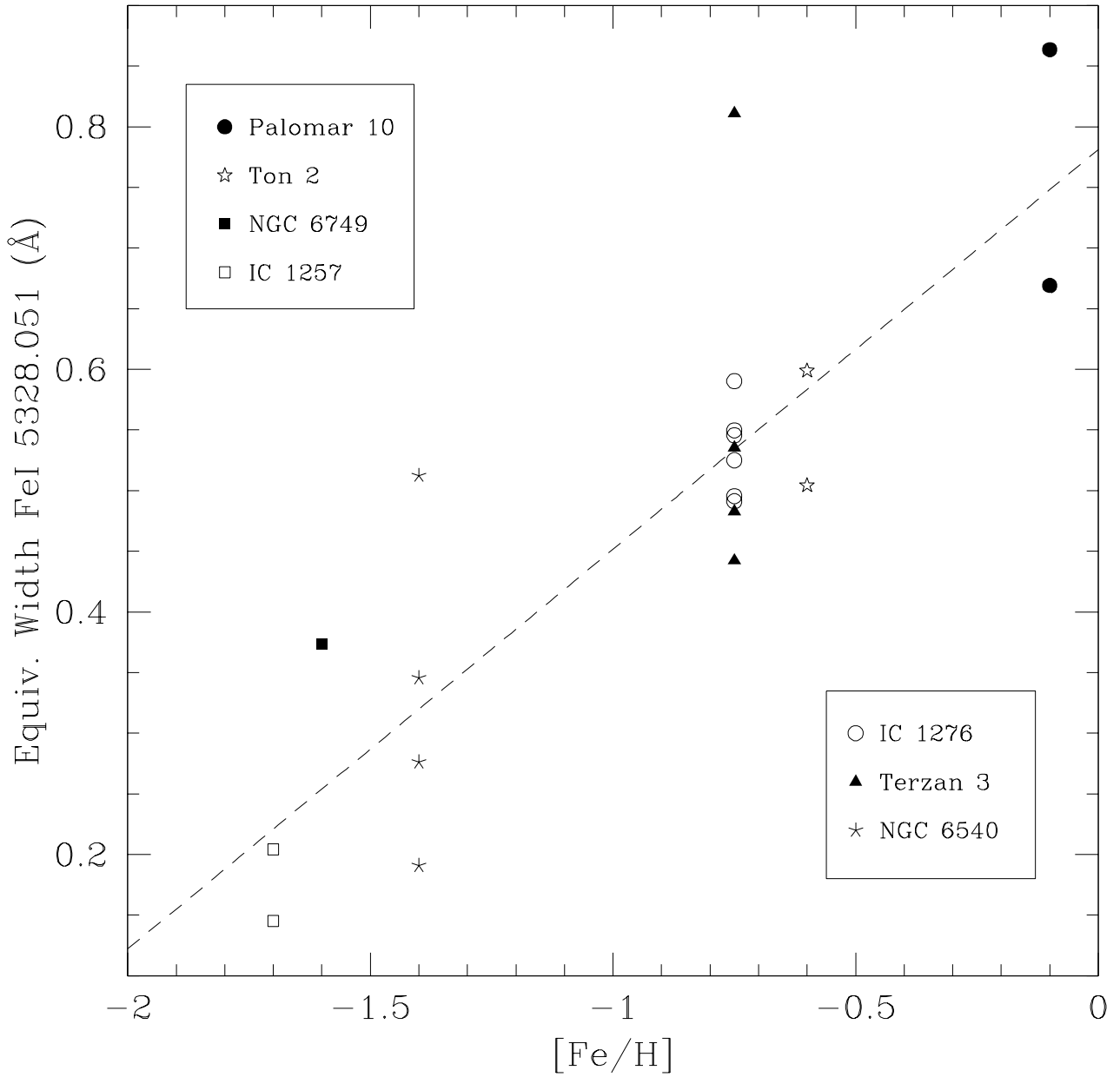


FIG. 7.— Equivalent width of the FeI 5328.051 Å line measured from our HIRES spectra plotted against published [Fe/H] for red giant stars in Pal 10, Ton 2, IC 1257 and NGC 6749. The dashed line shows the least-squares fit to the two quantities. Based on this relation, we estimate $[\text{Fe}/\text{H}] \sim -0.75 \pm 0.30$ for Terzan 3, $[\text{Fe}/\text{H}] \sim -0.75 \pm 0.15$ for IC 1276, and suggest a downward revision of the adopted metallicity of NGC 6540 from $[\text{Fe}/\text{H}] = -1.0$ to -1.40 ± 0.25 .

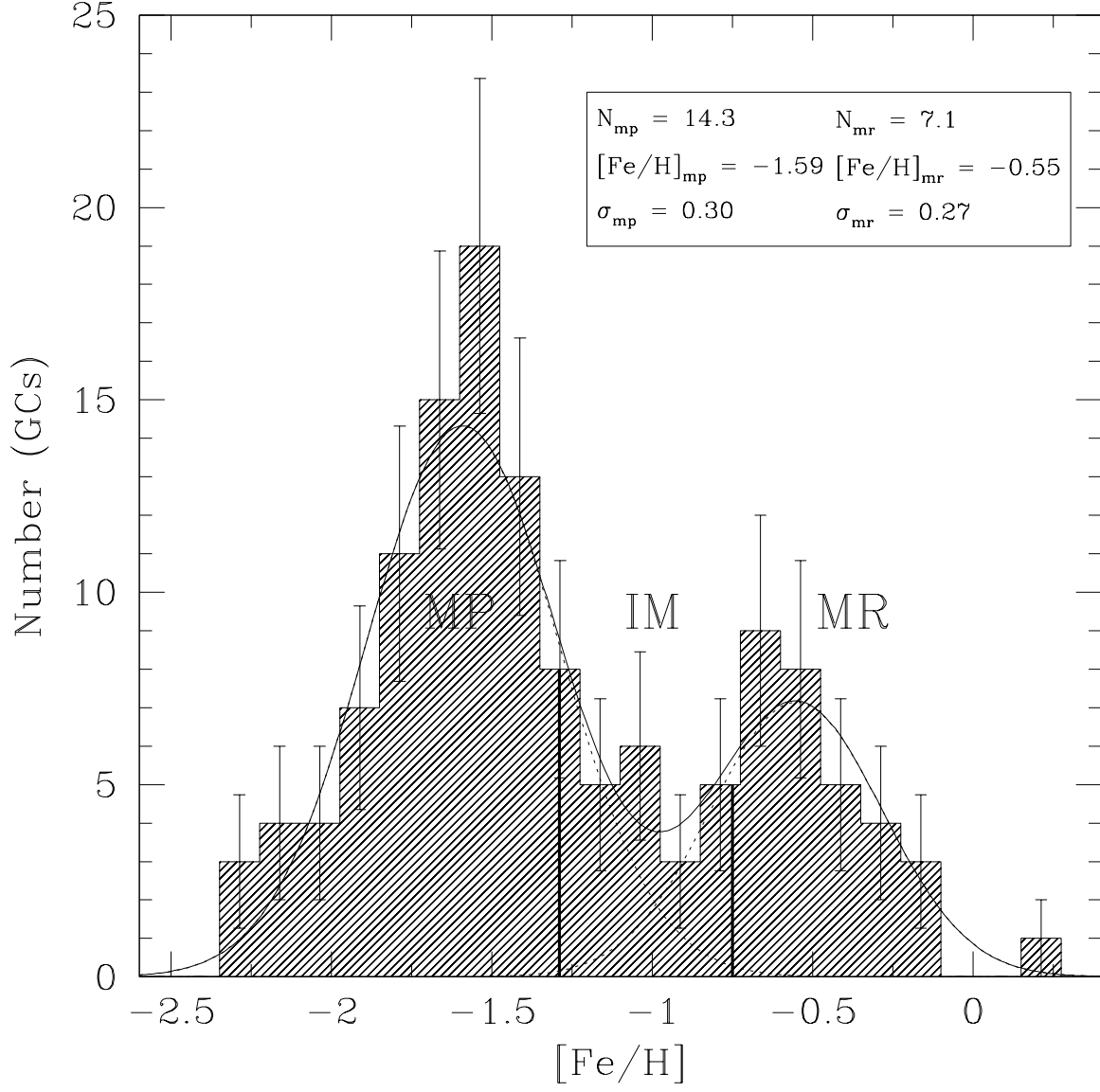


FIG. 8.— Histogram of 133 Galactic GCs having measured metallicities. The two-component Gaussian which best fits the observed distribution is shown as the solid line. The separate metal-rich and metal-poor components are indicated by the dotted lines. The heavy vertical lines at $[\text{Fe}/\text{H}] = -1.29$ and -0.75 show the boundaries used to define the samples of metal-rich (MR), metal-poor (MP) and intermediate metallicity (IM) clusters.

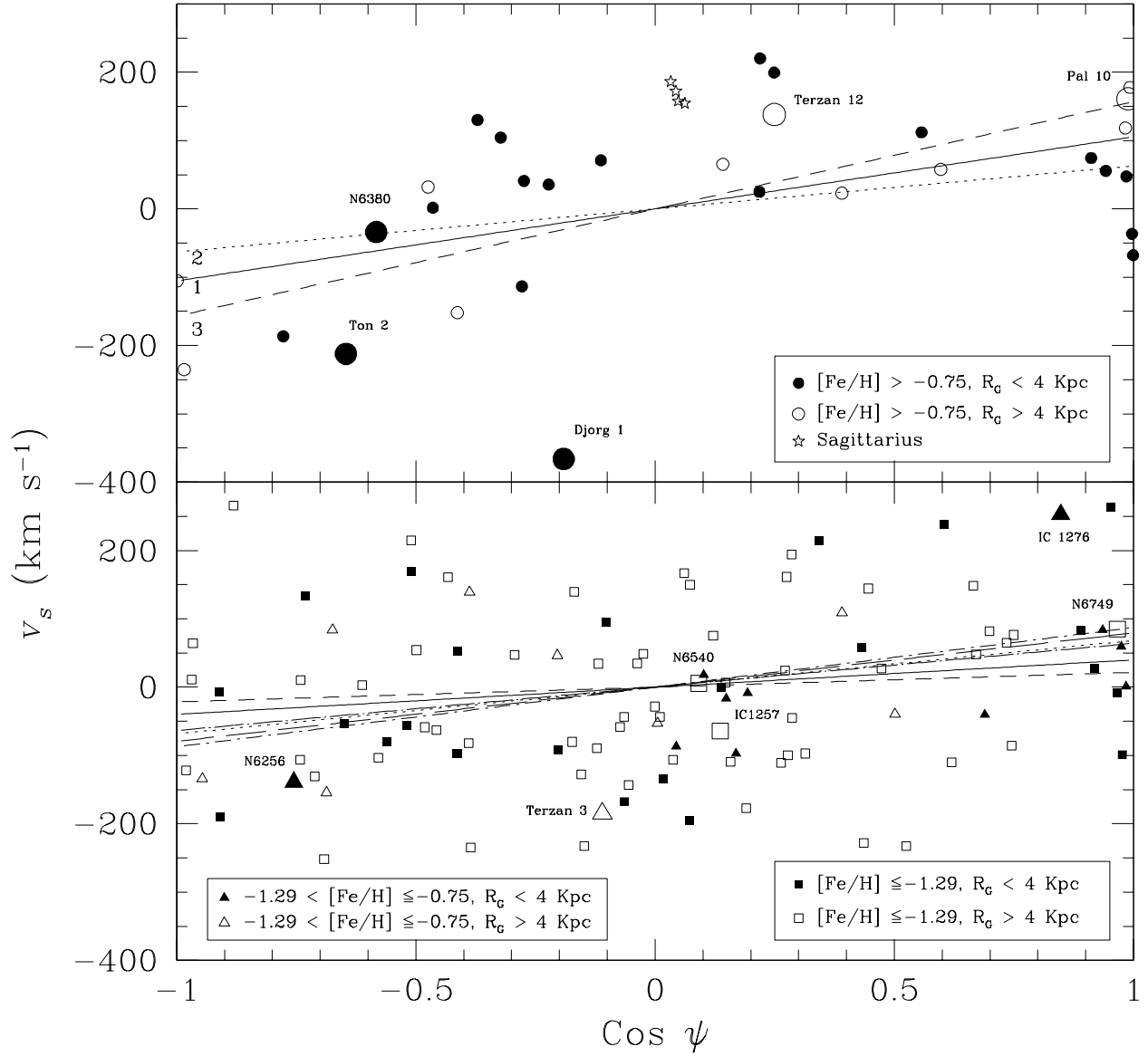


FIG. 9.— (Upper panel) Plot of v_s versus $\cos\psi$ for metal-rich GCs. Here ψ is the angle between the rotational-velocity vector of the cluster and the direction to the observer, and v_s is the velocity with respect to a stationary observer at the location of the Sun. Objects having a rotation velocity which is constant with Galactocentric radius should fall along a straight line in this diagram. The symbols are described in the keys to the figure. Small symbols refer to GCs taken from the catalog of Harris (1996); large symbols indicate clusters with radial velocities reported in this paper. The four probable or suspected members of the Sagittarius dwarf galaxy have been omitted from kinematic analysis of the Galactic GC system. The straight lines show the best-fit rotation solutions of the form of equation 3; each relation is numbered according to scheme given in Table 4. (Lower Panel) Same as above, except for metal-poor GCs (squares) and intermediate metallicity GCs (triangles).

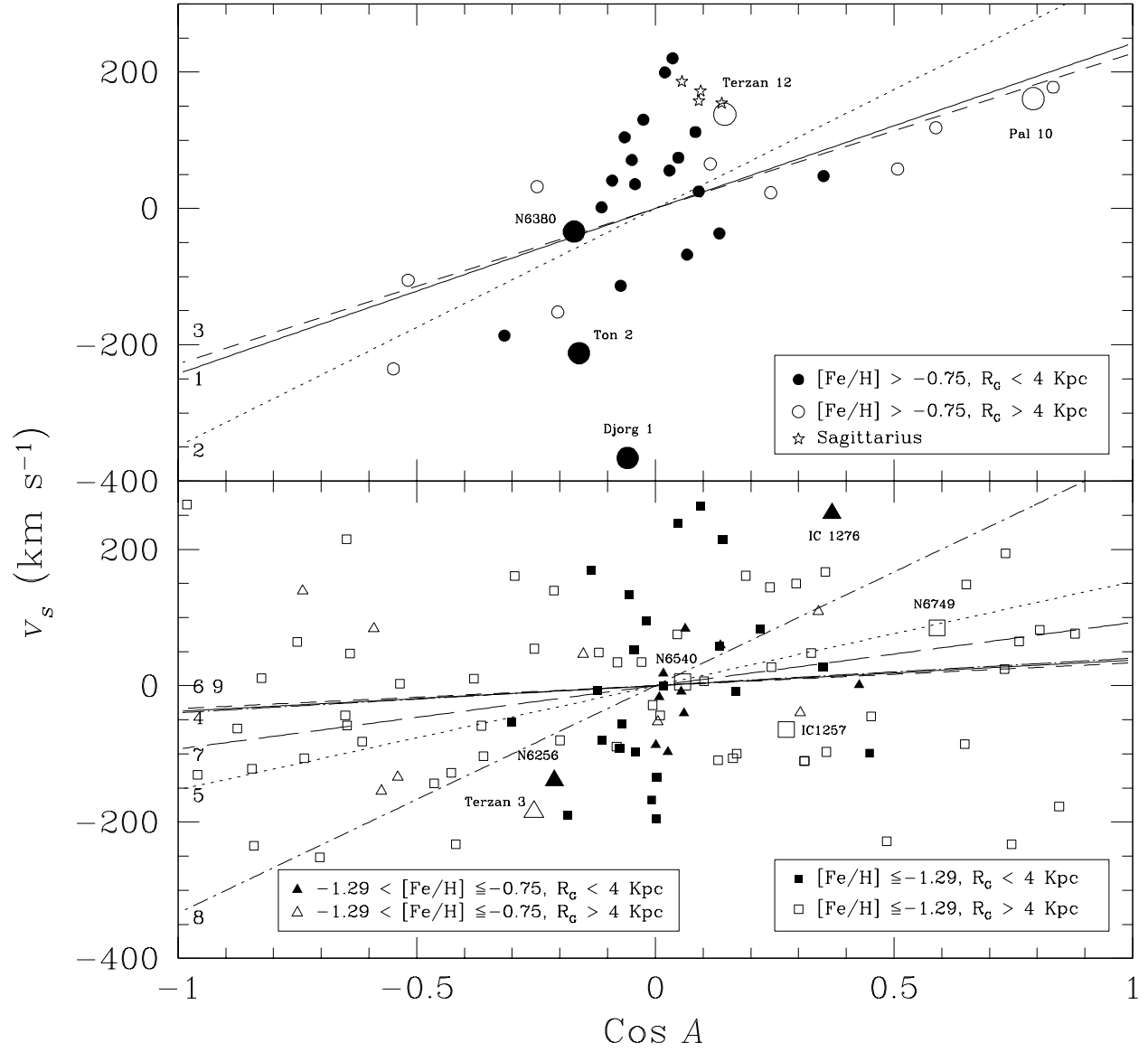


FIG. 10.— (Upper Panel) Plot of v_s versus $\cos A$ for Galactic GCs, where A is the angle between the apex of the Local Standard of Rest and the cluster's position on the sky. The symbols are the same as in Figure 9. Objects exhibiting solid-body rotation should fall along a straight line in this diagram. (Lower Panel) Same as above, except for metal-poor GCs (squares) and intermediate metallicity GCs (triangles).

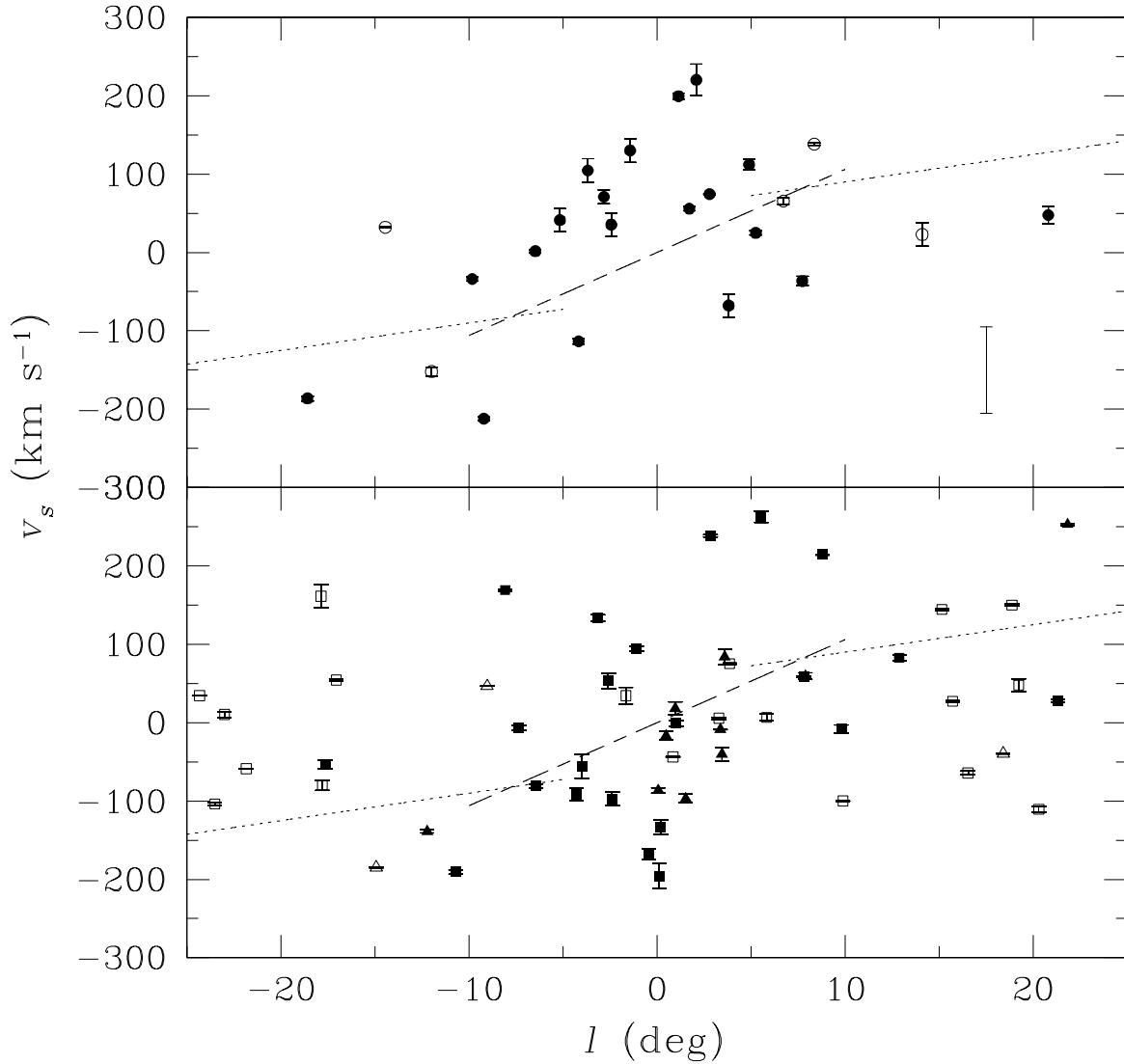


FIG. 11.— (Upper Panel) v_s plotted against Galactic longitude for metal-rich GCs. Open circles indicate GCs having $R_G \geq 4$ kpc; filled circles depict GCs having $R_G < 4$ kpc. The dashed line shows the rotation law for inner bulge stars reported by Tiede & Terndrup (1997). The dotted lines indicate the outer bulge rotation of $\sim 25 \text{ km s}^{-1} \text{ kpc}^{-1}$ found by Ibata & Gilmore (1995), shifted by $\pm 55 \text{ km s}^{-1}$ to match the inner relation of Tiede & Terndrup (1997). The errorbar shows the typical velocity dispersion of bulge objects (Kent 1992). (Lower Panel) v_s plotted against Galactic longitude for metal-poor GCs (squares) and intermediate metallicity GCs (triangles). Open symbols refer to GCs having $R_G \geq 4$ kpc; filled symbols indicate GCs having $R_G < 4$ kpc.

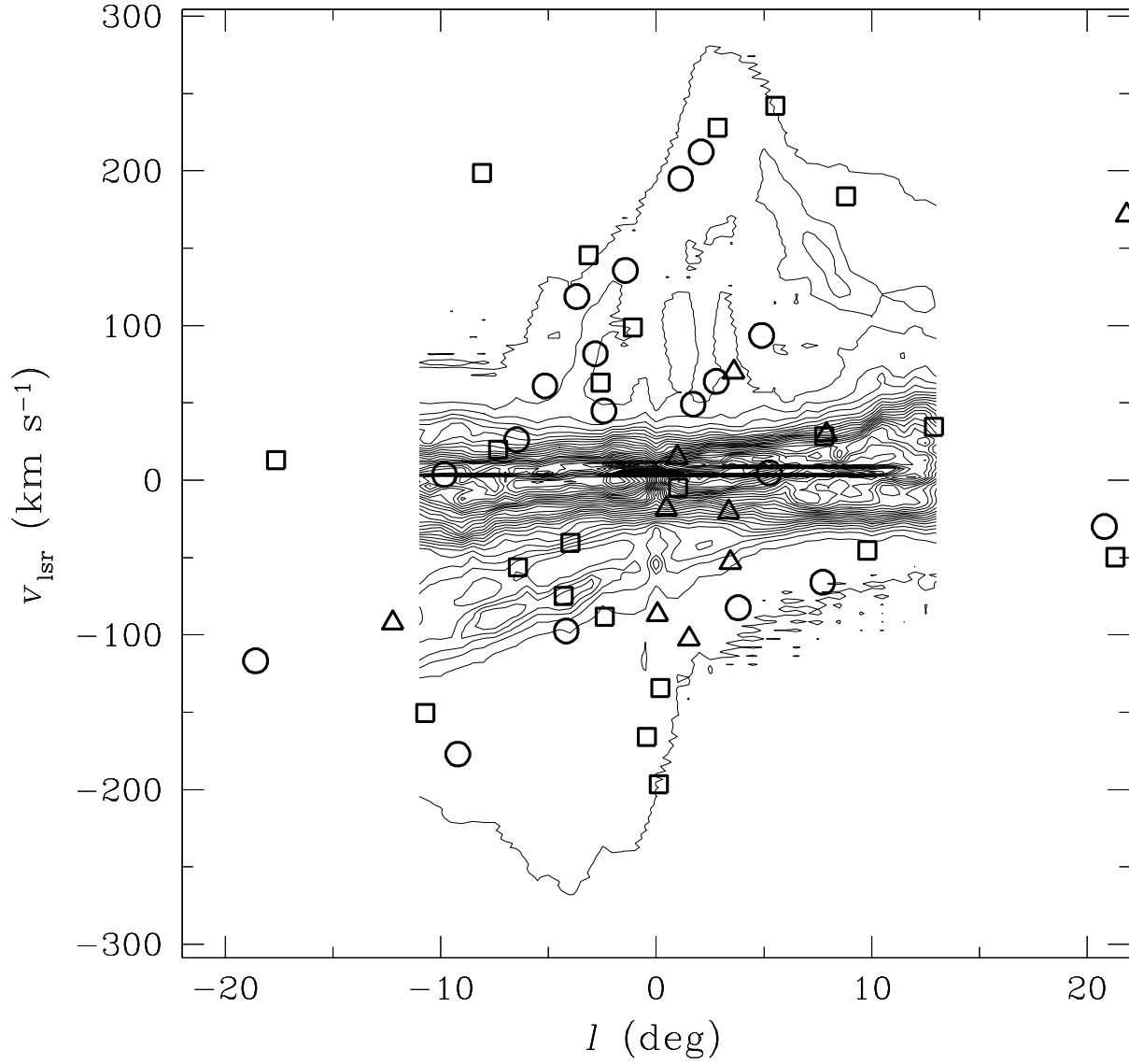


FIG. 12.— Longitude-velocity diagram in the direction of the Galactic center. The contours indicate the HI data of Burton & Liszt (1983), summed over the interval $|b| \leq 1.5^\circ$. Metal-rich GCs are indicated by circles, metal-poor GCs by squares and intermediate-metallicity GCs by triangles. With the exception of Djorg 1 (see text), all GCs within 4 kpc of the Galactic center are shown on this figure. The metal-poor cluster at $l \simeq -8^\circ$ and $v_{\text{lsr}} \simeq 200 \text{ km s}^{-1}$ is NGC 6144.

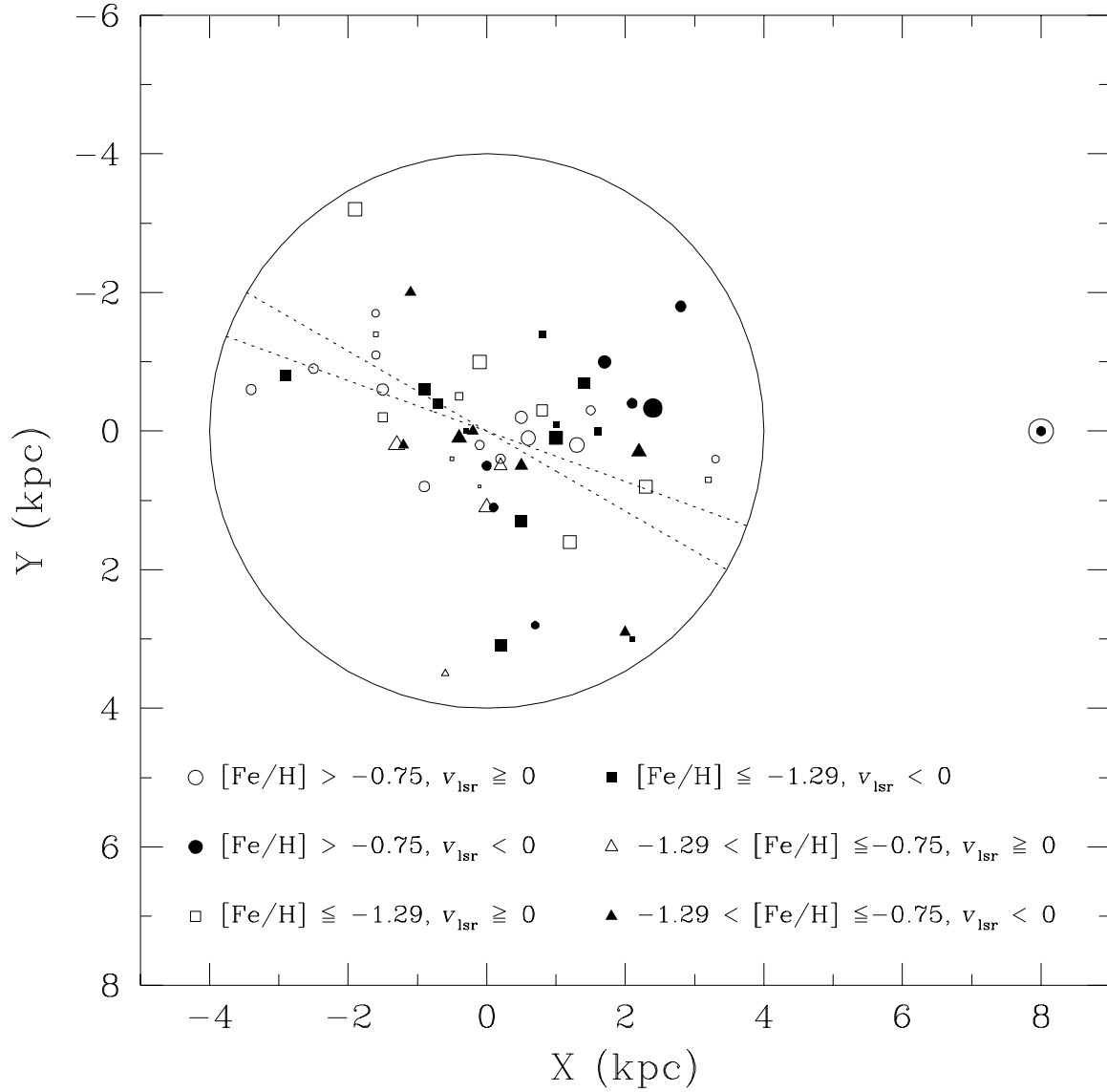


FIG. 13.— Distribution of all GCs within 4 kpc of the Galactic center having measured radial velocities. Metal-rich GCs are indicated by circles, metal-poor GCs by squares and intermediate-metallicity GCs by triangles. Open and filled symbols indicate GCs having $v_{\text{lsr}} \geq 0$ and $v_{\text{lsr}} < 0$, respectively. The size of the symbol is proportional to the absolute value of the observed velocity. The position of the sun is indicated at (8,0). The large circle with radius 4 kpc shows the approximate co-rotation radius of the Galactic bar (Fux 1997), while the two dotted lines indicate the limits on the orientation of the Galactic bar based on observations of red clump giants (Stanek et al. 1997).